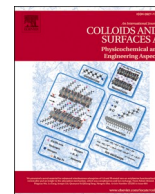


Contents lists available at [ScienceDirect](https://www.sciencedirect.com)

Colloids and Surfaces A: Physicochemical and Engineering Aspects

journal homepage: www.elsevier.com/locate/colsurfa

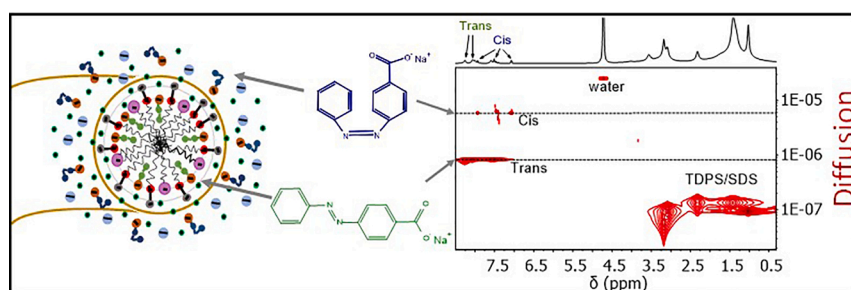
Selective incorporation of one of the isomers of a photoswitchable molecule in wormlike micelles

Natalia Rincón-Londoño^a, Cristina Garza^a, Nuria Esturau-Escofet^b, Anna Kozina^b, Rolando Castillo^{a,*}

^a Instituto de Física, Universidad Nacional Autónoma de México, P. O. Box 20-364, 01000, Mexico City, Mexico

^b Instituto de Química, Universidad Nacional Autónoma de México, P. O. Box 70-213, 04510, Mexico City, Mexico

GRAPHICAL ABSTRACT



ARTICLE INFO

Keywords:

Wormlike micelles
UV-irradiation
Photoswitchable molecules
Wormlike rheological properties
Wormlike micro-rheology
DOSY NMR

ABSTRACT

Understanding the physical and chemical mechanisms underlying the interactions between giant micelles and photoswitchable molecules is essential because it is not evident why some photoswitchable chromophores with apparently good potential to modify micellar systems' macroscopic properties have a poor performance on UV-irradiation. We report a mechanism that describes the trans-isomer's expulsion embedded in the wormlike micelles when it is transformed into the cis-isomer on UV-irradiation. Consequently, a small change in the rheological properties of the micellar solution is observed on UV-irradiation. As a model system, 4-(phenylazo) benzoate ion as the photoresponsive chromophore and giant cylindrical micelles made of N-Tetradecyl-N,N-Dimethyl-3-ammonio-1-PropaneSulfonate, and Sodium Dodecyl Sulfate, in saline water, are used. The trans-isomer chromophore incorporates into the micelles modifying the solution viscosity and viscoelastic spectra, which follows the Maxwell model at low and intermediate frequencies. However, the effect of UV-irradiation on rheological properties is not significant. Micro-rheological experiments are performed with diffusive wave spectroscopy to obtain high-frequency viscoelastic spectra to estimate the characteristic length scales of the wormlike micellar network with the embedded chromophore to understand its rheological behavior better. Detailed interaction between the chromophore and the micelles is obtained with ¹H-NMR and ¹H DOSY NMR experiments to determine the chromophore conformation into the micelles and diffusivity of the isomers.

* Corresponding author.

E-mail address: rolandoc@fisica.unam.mx (R. Castillo).

<https://doi.org/10.1016/j.colsurfa.2020.125903>

Received 8 June 2020; Received in revised form 15 October 2020; Accepted 6 November 2020

Available online 21 November 2020

0927-7757/© 2020 Elsevier B.V. All rights reserved.

1. Introduction

Surfactants can spontaneously self-assemble in different morphologies such as spherical micelles, Wormlike Micelles (WLMs), vesicles, lamellas, etc. Each morphology depends on the spontaneous curvature produced by the surfactants forming those aggregates, which in turn is determined by their packing factors that can be modified by surfactant concentration, temperature, ionic strength, or pH [1]. WLMs are long tubular flexible aggregates with end-caps, which have a curvature larger than in the cylindrical body. WLM size is the result of a balance between two contributions, the scission energy (energetic term) and the number of micelles (entropic term); although, there are other contributions to entropy due to tubular conformations and branching. These aggregates in the liquid where they are embedded usually form a network, which provides to those liquids with unique viscoelastic properties [2,3]. These properties enable them to be used in a wide range of applications, such as in oil fields, drag reduction, home care products, etc [4].

Several self-assembly systems have been reported with the ability to respond to external stimuli. These stimuli can be a change of temperature, light irradiation, pH, or electric field that generate a structural change [5]. These systems, named smart materials, can be used in applications related to change of surface wettability [6], drug delivery [7], the self-assembly or disassembly of structures, and molecular motors [8]. In the case of WLMs with an embedded photochromic switch, they can undergo a structural transition when exposed to UV-light. In particular, azobenzene derivatives are photoswitchable molecules presenting a trans-cis isomerization when they are UV-irradiated. The energy difference between the trans- and cis- isomer is $\sim 12 \text{ kcal mol}^{-1}$. The trans-isomer is more stable and predominant at room temperatures [9,10]. Azobenzene derivatives, which are incorporated into WLMs, can change the rheological properties of the micellar solution when exposed to UV-light because the trans-cis transition induces a change in the packing factor, and consequently, the spontaneous curvature of aggregates. Bi et al. [11] reported an increment in the contour length and entanglement in a micellar system with an azobenzene surfactant compound when the solution is UV-irradiated. The higher the irradiation time, the longer the WLMs; consequently, the system viscosity increases. Takahashi et al. reported another surfactant solution with azobenzene [12] that shows a viscosity change attributed to a transition from small micelles to WLMs after UV-irradiation. Yan et al. [13] also shows a transition from wormlike to spherical micelles on irradiation, with a significant decrease in viscosity. Recently, a chromophore (4-(phenylazo) benzoate ion) was embedded in cylindrical micelles made of CetylTrimethylAmmonium Bromide (CTAB) and Sodium Salicylate (NaSal) in water [14]. Here, with micro-rheology, it was determined that viscosity decreases as the chromophore concentration increases because the micellar length decreases. The chromophore makes the fluids more Maxwellian, and the viscoelastic spectra are modified. However, when the viscoelastic spectra are properly rescaled, they could be superimposed. However, the rheological change after UV-irradiation is not significant.

This paper presents a study of how a small chromophore, 4-(phenylazo)benzoate ion (PhazoBCOO⁻) capable of UV-light induced trans-cis isomerization, interacts with giant cylindrical micelles made of N-Tetradecyl-N,N-Dimethyl-3-ammonio-1-PropaneSulfonate (TDPS), and Sodium Dodecyl Sulfate (SDS) in saline water. This isomerization is one of the cleanest known photoreactions since no side-products are generated. Nevertheless, on a molecular scale, it leads to considerable changes in conformation and size. In contrast with numerous studies where photoswitchable molecules are mixed with micelles made of cationic surfactants, we discuss the interactions between micelles made of a mixture of an anionic and a zwitterionic surfactant and the mentioned azobenzene-based ion. The most relevant questions are the following: When the chromophore is added to the micellar solution, Does it incorporate into the WLMs? Are the length scales of the original WLM network modified? Is the chromophore able to alter the rheology

of the system on UV-irradiation due to the trans-cis isomerization?

In most papers dealing with incorporating photoswitchable compounds, authors report how UV-irradiation modifies their systems' behavior. However, there are much fewer reports about what occurs in systems that it does not work, despite containing photoswitchable molecules, as in the present system. Although the solutions self-assemble in WLMs when a photoswitchable molecule is added, and their rheological properties are modified, the change of their macroscopic properties is not significant on UV-irradiation. As we will see further, the clue of what is occurring during the UV-irradiation in the present micelle solution can be provided by ¹H-NMR experiments. Thus, understanding the system's physical chemistry is essential to explain why some chromophores with apparently good potential have a poor performance. As mentioned above, in some cases, on UV-irradiation, WLMs are disassembled, or the micelles' size is dramatically reduced. Thus, a significant change in rheological behavior ensues. Here, we present a different mechanism. We are confident that much can be learned and used to design new photoswitchable mixtures, studying the chromophore-micelle interactions and how isomerization processes occur.

2. Material and methods

2.1. Materials

Sodium Dodecyl Sulfate (SDS, purity $\geq 99\%$) comes from Merck (Germany), 4-(phenylazo) benzoic acid (PhazoBCOO⁻ H⁺, purity $> 98\%$) are from TCI Tokyo Chemical (Japan). N-tetradecyl-N,N-dimethyl-3-ammonio-1-propanesulfonate (TDPS, purity $\geq 99\%$), sodium chloride (NaCl, purity $> 99\%$), Sodium hydroxide (NaOH, purity $\geq 97\%$), and D₂O (99.9%) are from Sigma-Aldrich (Canada). All chemicals were used as received. Ultrapure deionized water (Nanopure, USA) was used to prepare the samples.

2.2. Sample preparation

PhazoBCOO⁻ H⁺ was solubilized in deionized water at $pH = 12$, with the aid of a NaOH solution to obtain PhazoBCOO⁻. Samples were stirred and heated up to 40°C , then TDPS and SDS were added to maintain a constant ratio of $R = 0.55$ ($R = [SDS]/[TDPS]$) with $[TDPS] = 46 \text{ mM}$. NaCl was added to all samples to reach 0.5 M . After stirring the mixtures for 24 h , they were left to relax for 48 h . The PhazoBCOO⁻ concentration, C_{AZO} , in the studied micellar solutions are $C_{AZO} = 5, 10, 20, \text{ and } 30 \text{ mM}$. Micellar solutions without PhazoBCOO⁻ were also prepared, following the same method, to be used as a reference.

2.3. UV-light irradiation

A 365 nm LED-array light source (31 mW , LUI365A, Thorlabs, USA) was used for irradiating samples for 1 h before the tests, as well as during the rheological measurements. PhazoBCOO⁻ Na⁺ ($3 \times 10^{-4} \text{ M}$) UV-vis spectrum in water solution at $pH = 12$ presents two transitions, like other azobenzene derivatives. A first one, $\pi \rightarrow \pi^*$, occurs at 325 nm , and a second one, $n \rightarrow \pi^*$, occurs at 420 nm . When the sample is UV-irradiated, the band at 325 nm decreases, and the other one at 420 nm slightly increases. On white light irradiation, the transition goes backward; although, it does not reach the sample's initial absorbance without any previous irradiation. The absorption spectrum of PhazoBCOO⁻ can be found in Ref. [14].

2.4. ¹H-NMR and ¹H diffusion-ordered spectroscopy (DOSY) NMR

A Bruker AVANCE III HD 500 MHz spectrometer (USA) with a 5-mm double resonance broadband (BBFO) probe was employed to obtain the NMR spectra. This instrument is also equipped with a z-gradient coil capable of generating maximum field strengths of 50 G cm^{-1} ; standard Bruker pulse sequences were used. For the measurement of diffusion, the

^1H DOSY NMR experiments were developed using a standard bipolar gradient pulse sequence for diffusion measurement with a double stimulated echo for convection compensation and LED (longitudinal eddy current delay) with three spoil gradients. The diffusion time was 100 ms, with a LED delay of 5 ms. Smooth-square-shaped gradient pulses were used for the experiments, with a duration of 3 ms ensued by a recovery delay of 200 μs , with 32 equal increments in a range from 5 % to 95 % of the maximum strength. A measurement of the self-diffusion coefficient of the residual HDO signal in a D_2O sample at 25 $^\circ\text{C}$, helped to calibrate the gradient strength. For the maximum gradient strength's back-calculation, a value of $1.90 \times 10^{-9} \text{ m}^2\text{s}^{-1}$ was used. In all NMR spectra, Fourier transformation was done using a 1 Hz line broadening and baseline correction. ^1H DOSY spectrum was analyzed, selecting a mono-exponential function, with the Bruker Topspin software package. Samples were prepared in D_2O (99.9 %) and NaOD, and NMR spectra were referenced to the water signal resonance for each temperature.

2.5. Rheological measurements

Rheological measurements were performed with a MCR-702 Twin-Drive rheometer (Anton Paar, Austria). Flow curves and viscoelastic measurements were carried out using a cone-plate geometry (2° cone angle, Diam. = 40 mm) with temperature control (± 0.1 $^\circ\text{C}$). The oscillatory experiments were obtained in the linear regime. A solvent trap was used to avoid water evaporation, provided with a quartz window to keep the sample UV-irradiated during the measurements.

2.6. Microrheology and diffusive wave spectroscopy (DWS)

DWS is a technique used to measure the Mean Square Displacement (MSD), $\langle \Delta r^2(t) \rangle$, of microspheres embedded in a complex fluid. The MSD is connected to $G^*(\omega)$ through the generalized Stokes-Einstein equation, by Mason and Weitz: [15]

$$G^*(\omega) = G'(\omega) + iG''(\omega) = \frac{k_B T}{\pi r_o i \omega \mathfrak{S}[\langle \Delta r^2(t) \rangle]} \quad (1)$$

Here, $\mathfrak{S}[\]$ represents a unilateral Fourier transform, ω is the angular frequency, the microsphere radius given by r_o , T is the temperature, and k_B is the Boltzmann constant. With this technique, the viscoelastic spectrum of WLM solutions can be extended to high frequencies ($\sim 10^6 \text{ rad s}^{-1}$).

The MSD of microspheres is determined, collecting their scattered light from a single speckle, during an extended period where the time-averaged intensity auto-correlation function is measured. Microspheres embedded in the micellar liquid are placed in a cuvette with an optical path length $L \gg l^*$, with an essentially infinite transverse extent, [16] where l^* is the light's transport mean free path. The fluid without probe particles must be entirely transparent to the incident light beam in the standard DWS, but micellar solutions with azocompounds absorb light. Notwithstanding, it is possible to include a correction using the Inverse Adding-Doubling method (IAD) [17,18], which is a method developed to recover the optical parameters like the absorption length l_a and l^* . These parameters can be determined from three measurements: total reflectance, total transmittance, and collimated transmittance of light. The MSD of the tracers can be obtained from the corrected intensity autocorrelation function, due to including l_a [19]. The MSD curves determined for the microspheres immersed in the micellar solutions are best fitted with a model curve given by Bellour et al. [20]:

$$\langle \Delta r^2(t) \rangle = 6\delta^2 \left(1 - e^{-\left(\frac{D_0}{\delta^2} t\right)^\alpha} \right)^{\frac{1}{\alpha}} \left(1 + \frac{D_m}{\delta^2} t \right) \quad (2)$$

Here, the plateau of $\langle \Delta r^2(t) \rangle$ vs. t curve is measured by $6\delta^2$; D_0 , and D_m are the diffusion coefficients for microspheres in the solvent at infinite

dilution and at long times, respectively. The components of $G^*(\omega)$ are obtained using the fitting curves in Eq. (1). From $G^*(\omega)$, the essential characteristic lengths of the WLM network can be obtained. At high frequencies, the Maxwellian stress relaxation processes are frozen, and $G^*(\omega)$ exhibits a power-law behavior, $|G^*(\omega)| \sim \omega^\nu$, with an exponent $\nu \sim 5/9$ in the Rouse-Zimm regime, which changes to $\nu \sim 3/4$. This occurs because now, the WLMs behave like semiflexible polymer chains, and the internal bending modes of Kuhn segments dominate. The change occurs at a frequency $\omega_0 \approx k_B T / (8\eta_s l_p^3)$. Here, η_s is the solvent viscosity, and l_p is the persistence length [21] that corresponds to the shortest relaxation time in the Rouse-Zimm spectrum. From ω_0 coming from the mentioned slope change in $|G^*(\omega)|$, l_p and other characteristic lengths can be found to comprehend and evaluate the structure and dynamics of WLMs. In the loose entanglement regime, the WLM network mesh size,

ξ , can be estimated using $\xi \cong \left(A \frac{k_B T}{G_0} \right)^{1/3}$; here, the prefactor $A = 9.75$ is a correction introduced recently [22]. The entanglement length, l_e , can be calculated using $l_e = \xi^{5/3} / l_p^{2/3}$ [23]. The total contour length, L_C , can be predicted from $G''_{min}/G_0 \cong \left(l_e/L_C \right)^{0.8}$ that comes from incorporating breathing and high-frequency Rouse modes; the exponent is a correction given by Granek [24]. G''_{min} is the local minimum of $G''(\omega)$ after the first crossing between the $G'(\omega)$ and $G''(\omega)$ moduli. The entanglement length to the persistence length ratio, $\alpha_e = l_e/l_p$, can be also evaluated, which is useful to determine if the system is in the loose ($\alpha_e > 2$) or tight ($\alpha_e < 1$) entanglement regime [22].

3. Results and discussion

TDPS/SDS in saline water self-assemble in WLMs as determined by Small-Angle Neutron Scattering (SANS), [25] and they are stable enough to include a small chromophore as PhazoBCOO $^-$ into the micelle, without deforming the tubular structure significantly. Fig. 1 shows negative staining micrographs obtained by Scanning Electron Microscopy (SEM) of dilute micellar solutions (\sim overlap concentration $\sim 9 \text{ mM}$ in TDPS), where long tubular structures are easily observed. Their diameter is on the average $\sim 3.7 \text{ nm}$, similar to those WLMs without adding the chromophore ($\sim 3.38 \text{ nm}$) using the same technique [25]. The measured diameter of the micelles of this system without chromophore is 4.7 nm employing SANS [25]. Birefringence appears when the micellar solutions with PhazoBCOO $^-$ are sheared (not shown), which is also a typical behavior of WLM solutions. As we will see below, the rheological measurements (Cole-Cole plots) are also consistent with the fact that the micelles with the chromophore are WLMs.

3.1. Rheology

Fig. 2a shows the viscoelastic spectra of WLM solutions as a function of the azobenzene concentration before and after UV-irradiation (inset Fig. 2a). The crossing points, G_c and ω_c , between $G'(\omega)$ and $G''(\omega)$ for all the PhazoBCOO $^-$ concentrations can be found at $3.98 < G_c < 7.54 \text{ Pa}$ and $0.014 < \omega_c < 0.089 \text{ s}^{-1}$. For micellar solutions with $5 < C_{AZO} < 20 \text{ mM}$, ω_c shifts to lower frequencies, and G''_{min} decreases. For $C_{AZO} = 30 \text{ mM}$, the spectra are shifted to higher frequencies; consequently, ω_c does the same. Here, G''_{min} is out of range of our mechanical measurements. When the viscoelastic spectra are normalized using their respective Maxwell parameters, i. e., dividing the modulus by $G_0 = 2G_c$ and multiplying the frequency by $\tau_0 = 1/\omega_c$, as shown in Fig. 2b, the crossing points are almost at the same positions for most of all the micellar solutions. The G''_{min} values are very similar for the solutions with $C_{AZO} = 5, 10, \text{ and } 20 \text{ mM}$ (Fig. 2a). On UV-irradiation, the micellar solutions do not show any significant change, as shown in the inset of Fig. 2a, as well as in the inset of Fig. 2b with normalized spectra for solutions with $C_{AZO} = 5 \text{ and } 10 \text{ mM}$, before and after UV-irradiation. Viscoelastic behavior

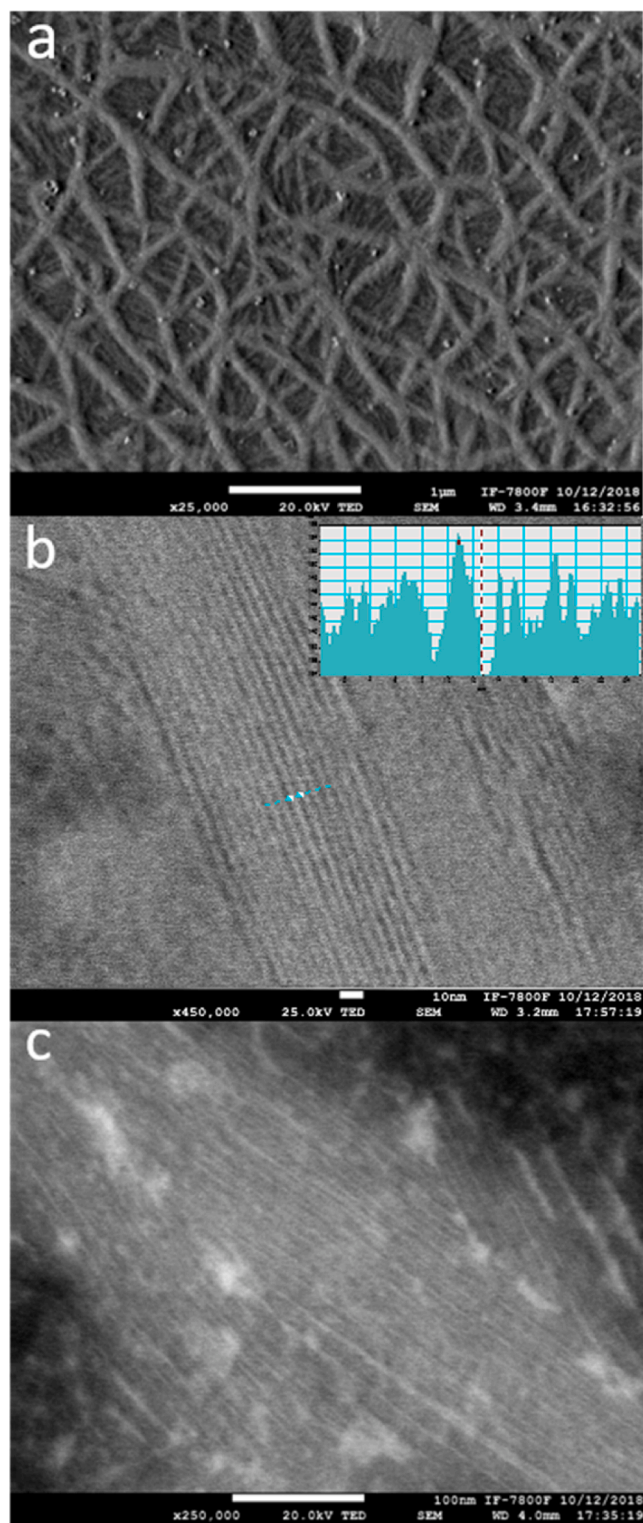


Fig. 1. Negative staining micrographs obtained by SEM of dilute micellar solutions of TDPS/SDS/NaCl with the chromophore, developed using phosphotungstic acid (1.5 %) [14]. Different amplification: a) 25,000X, bar =1 μm. b) 450,000X, bar = 10 nm. Here, a profile is included to estimate the micellar diameter; in this example, the indicated one was of 3.68 nm, and c) 250,000X, bar = 100 nm another sample with more chromophore (1.5 times more than in the previous micrographs).

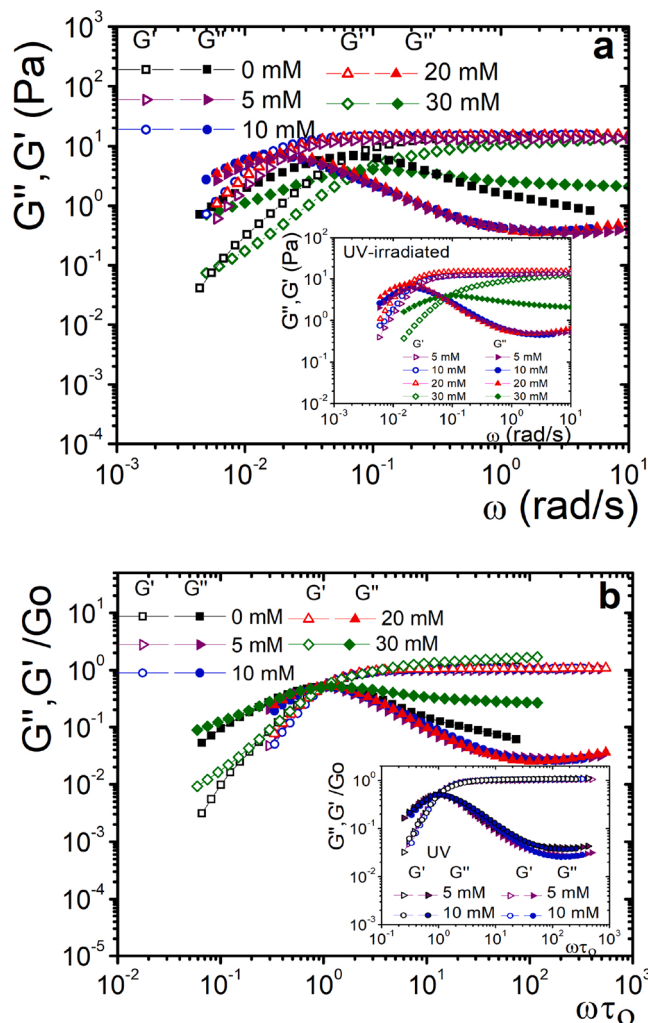


Fig. 2. Viscoelastic spectra for micellar solutions of TDPS/SDS/NaCl ($[TDPS] = 46 \text{ mM}$, $R = 0.55$) with different concentration of added PhazoBCOO⁻ ($C_{AZO} = 0, 5, 10, 20, \text{ and } 30 \text{ mM}$, $T = 25 \text{ }^\circ\text{C}$, $\text{pH} = 12$). a) Before and after UV-irradiation (inset). b) Normalized viscoelastic spectra for those given in (a); inset before and after UV-irradiation for $C_{AZO} = 5$ and 10 mM .

essentially does not change with irradiation, but G''_{min} increases a little. A similar UV-response result was obtained by Tu et al., [26] for wormlike micelles made of a Gemini surfactant and cinnamate. This result was attributed to the low trans-cis isomerization of the cinnamate. Fig. SM1 presents Cole-Cole plots for all the employed concentrations of PhazoBCOO⁻. They follow a semi-circle curve at low and intermediate frequencies, which indicates that the samples present a Maxwellian behavior. i. e., stress, σ , relaxes through one decaying exponential, $\sigma = G_0 e^{-t/\tau_0}$, where the relaxation time, τ_0 , is the geometric mean of the breaking-recombination and reptation times. The Maxwellian behavior coincides with the WLM structure observed in the SEM images. The solution with $C_{AZO} = 30 \text{ mM}$ does not follow the semi-circle shape at intermediate frequencies and large frequencies, indicating that the sample relaxes via different relaxation modes at such frequencies, as contour length fluctuations and Zimm-Rouse modes. Insets of Fig. SM1 show the Cole-Cole plots for the solutions before and after UV-irradiation for different chromophore concentrations. The samples irradiated still present a Maxwellian behavior; this indicates that the tubular structure of these micelles does not seem to change with UV-irradiation.

Fig. 3a shows the relaxation times, τ_0 , for the micellar solutions as a function of PhazoBCOO⁻ concentration before and after UV irradiation.

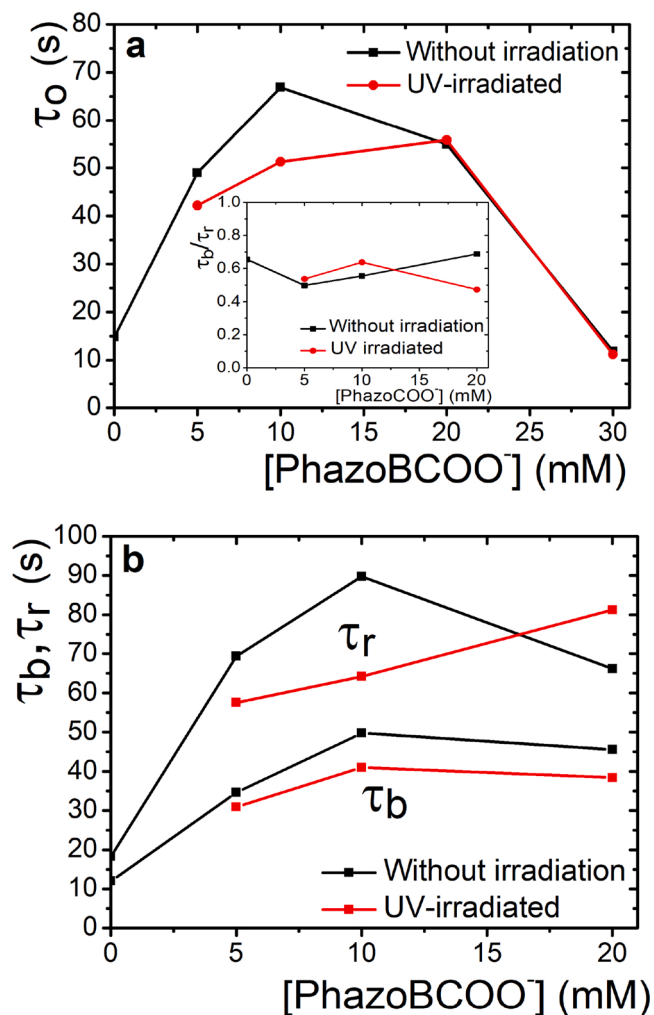


Fig. 3. Characteristic times for micellar solutions of TDPS/SDS/NaCl ([TDPS] = 46 mM, R = 0.55) as a function of added PhazoBCOO⁻, before and after UV-irradiation, at T = 25 °C and pH = 12. a) τ_0 vs. C_{AZO} . Inset $\zeta = \tau_b/\tau_r$ vs. C_{AZO} . b) τ_b and τ_r vs. C_{AZO} .

In the non-irradiated solutions, as we add the chromophore, we observe an increment of relaxation time until $C_{AZO} = 10$ mM is reached. After this concentration, relaxation times decrease. The increase is related to an increment in the micelles' total contour length, as we will show with the microrheological results presented below. The solution with $C_{AZO} = 30$ mM has almost the same relaxation time as the original micellar solution without PhazoBCOO⁻. When micellar solutions are UV-irradiated, for $C_{AZO} = 5$ and 10 mM, the relaxation times decrease comparing with the non-irradiated ones, but they do not change for the case of $C_{AZO} = 20$ and 30 mM. Fig. 3b presents the breaking-recombination (τ_b), and reptation (τ_r) times as a function of the PhazoBCOO⁻ concentration with and without UV-irradiation. We used the method given by Turner and Cates [27] for calculating τ_b and τ_r , and $\tau_0 \approx \sqrt{\tau_b \tau_r}$ and $\zeta = \frac{\tau_b}{\tau_r}$ [28]. For the micellar solution with $C_{AZO} = 30$ mM, it is not possible to calculate these characteristic times because its Cole-Cole plot does not cut the x-axis (see Fig. SM1), which is a condition needed in the mentioned method. Both characteristic times have similar behavior for non-irradiated solutions. They increase up to $C_{AZO} = 10$ mM, and afterward, they decrease. In the irradiated solutions, τ_r increases as the concentration increases and τ_b is not too sensitive to changes in concentration. The inset of Fig. 3a shows the ratio between τ_b and τ_r versus C_{AZO} . $\zeta = \tau_b/\tau_r$ indicates how good the Maxwellian behavior is, which must be $\zeta < 1$ and perfect when $\zeta \ll 1$. The values of ζ for all systems

before and after UV irradiation (excluding $C_{AZO} = 30$ mM) vary from 0.48 to 0.68. All these solutions behave as Maxwellian fluids.

3.2. Flow curves

Fig. 4a presents viscosity, η , vs. $\dot{\gamma}$ for the micellar solutions with $C_{AZO} = 0, 5, 10, 20,$ and 30 mM, before and after UV-irradiation. At low $\dot{\gamma}$, the viscosity is approximately constant or with a small shear thinning. Viscosity increases for the solutions with $C_{AZO} = 5, 10,$ and 20 mM with respect to $C_{AZO} = 0$ mM. At $C_{AZO} = 30$ mM, viscosity is similar to the solution without chromophore. Viscosity vs. C_{AZO} graphs follow the same trend as the plot of τ_0 vs. C_{AZO} . At some specific value of $\dot{\gamma}$, all solutions present a strong shear thinning behavior before and after UV-irradiation, similar to the case when shear banding is present. Below, we will show that, indeed, it is the case, and this is because the slopes of the flow curves almost collapse on a single curve (slope ~ -0.96 mPa s²). Fig. 4b shows the normalized shear stress, σ/G_0 , as a function of the normalized shear rate, $\dot{\gamma} \tau_0$, for these solutions. All solutions have similar behavior, although, for the case of $C_{AZO} = 5, 10,$ and 20 mM, they behave notoriously alike. For $C_{AZO} = 0$ and 30 mM, they have a shorter horizontal plateau. At low shear rates, all curves show a linear behavior,

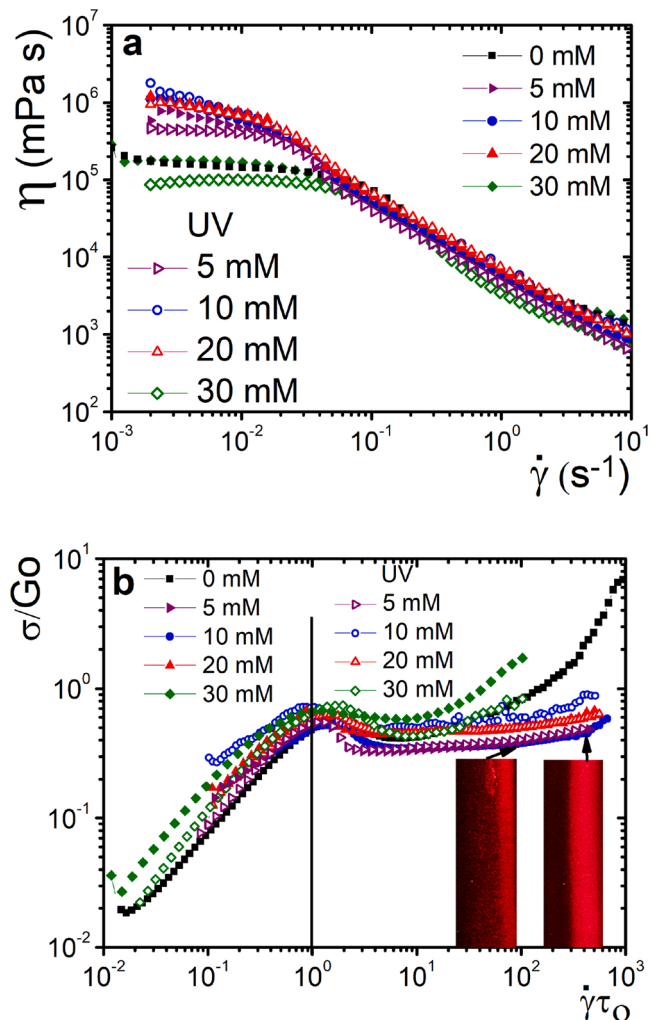


Fig. 4. Flow curves for the micellar solutions of TDPS/SDS/NaCl ([TDPS] = 46 mM, R = 0.55) with $C_{AZO} = 0, 5, 10, 20,$ and 30 mM, before and after UV-irradiation. a) η vs. $\dot{\gamma}$. b) σ/G_0 vs. $\dot{\gamma} \tau_0$. Shear banding starts after $\dot{\gamma} \tau_0 = 1$, marked with a vertical black line. Inset: images of the shear bands for the micellar solution with $C_{AZO} = 10$ mM obtained with the aid of a sheet of light along the gradient direction. Left image at $\dot{\gamma} = 2$ s⁻¹, and right image at $\dot{\gamma} = 6.2$ s⁻¹.

and after a small shear-thickening peak around $Wi = \dot{\gamma} \tau_o \sim 1$, $\sigma/G_o(\dot{\gamma}\tau_o)$ is almost constant. Wi is the Weissenberg number, an adimensional number that compares the elastic forces to the viscous forces in a fluid. The plateau corresponds to a nonequilibrium phase transition forming bands in the gradient direction, between an isotropic phase of randomly oriented micelles and a paranematic phase with oriented micelles in the direction of flow [29]. The shear bands can be observed in the insets of Fig. 4b for a micelle solution with $C_{AZO} = 10$ mM. The bands are obtained with the aid of a sheet of light along the direction of the gradient [32]. In the images, it can be observed as a glossy band corresponding to the paranematic phase and a dark band corresponding to the isotropic fluid. Similar shear banding was also found in the micellar solution without the chromophore at the same surfactant concentrations presented here, [30] as recently confirmed with SANS [25]. This nonlinearity arises from the coupling between flow and mesostructure, *i. e.*, flow reorganizes mesostructure, which feeds back on the flow. There are two branches in the constitutive curve in these systems, one at low and another at high shear rates. They are separated by an unstable mechanical regime where $\frac{d\sigma}{d\dot{\gamma}} < 0$. For an imposed shear rate, mechanical stability requires a separation of the fluid into bands due to the negatively slope regime in the constitutive curve; the instability triggers shear bands' formation [31].

3.3. Micro-rheology

In these experiments, negatively charged polystyrene microspheres ($Diam. = 800$ nm) are used as tracers, which are dispersed in the WLM solutions. The MSD of these embedded particles is measured with DWS. We measured the micellar solutions without UV-irradiation because PhazoBCOO⁻ absorb visible light in the wavelength range of the employed laser (514.5 nm) [14]. Fig. 5a shows the measured curves of MSD vs. t , and their fits to the Bellour model, [20] for WLM solutions with $C_{AZO} = 0, 5$, and 10 mM. For samples with $C_{AZO} = 20$ and 30 mM, we could not obtain the MSD due to the chromophore's high light absorption in the solutions. The experimental MSD vs. t curves were fitted to Eq. 2, where δ, D_m, D_o , and α are free parameters. At short times, the MSD is a linear function of time: $\langle \Delta r^2(t) \rangle = 6D_o t$. Here, D_o is the diffusion coefficient at high dilution. In these curves, an estimate of the network's average size (the cage size δ) can be given as a function of elastic modulus G_o ($6\delta^2 = k_B T / \pi r_o G_o$). The plateau is where microspheres are momentarily trapped before the network relaxes and, after relaxing, leave the microspheres to continue their motion. Now, the MSD again is a linear function of time, $\langle \Delta r^2(t) \rangle = 6D_m t$, where D_m is related to the viscosity of the solution η_m through $D_m = k_B T / 6\pi r_o \eta_m$. The microspheres' dynamics exhibit a broad time relaxation spectrum at the plateau onset time, leading to including the parameter α as given by Eq. 2. The MSD is related to $G^*(\omega)$ through a generalized Stokes-Einstein equation, Eq. 1. Fig. 5b,c, and the inset of Fig. 5c show the viscoelastic spectra obtained using mechanical rheology and microrheology for the micellar solutions with $C_{AZO} = 0, 5$, and 10 mM, respectively. Both spectra are similar, but there is a difference at the crossing point (G_c) values of viscoelastic spectra obtained through mechanical rheology and microrheology. The crossing points in the viscoelastic spectra obtained by micro-rheology moves to higher frequencies. There is a reasonable agreement for G_o ($G_o = 2G_c$) in both techniques. However, there is a difference of one order of magnitude in τ_o . In the WLM system without chromophore, it was reported that at shorter τ_o values, the deviation between both methods is more substantial [33]. On average, it was found a difference between DWS measurements with respect to mechanical rheometry of ~ 20 % for G_o , and ~ 35 % for τ_o . In general, when measured with DWS, the G_o and τ_o values are always lower than those measured with mechanical rheometry. The agreement between the measurements is reasonable in most of the cases, although it is not excellent. Comparing rheological data of WLMs obtained by different methods is not an easy task because protocols play a central role. In particular, in mechanical

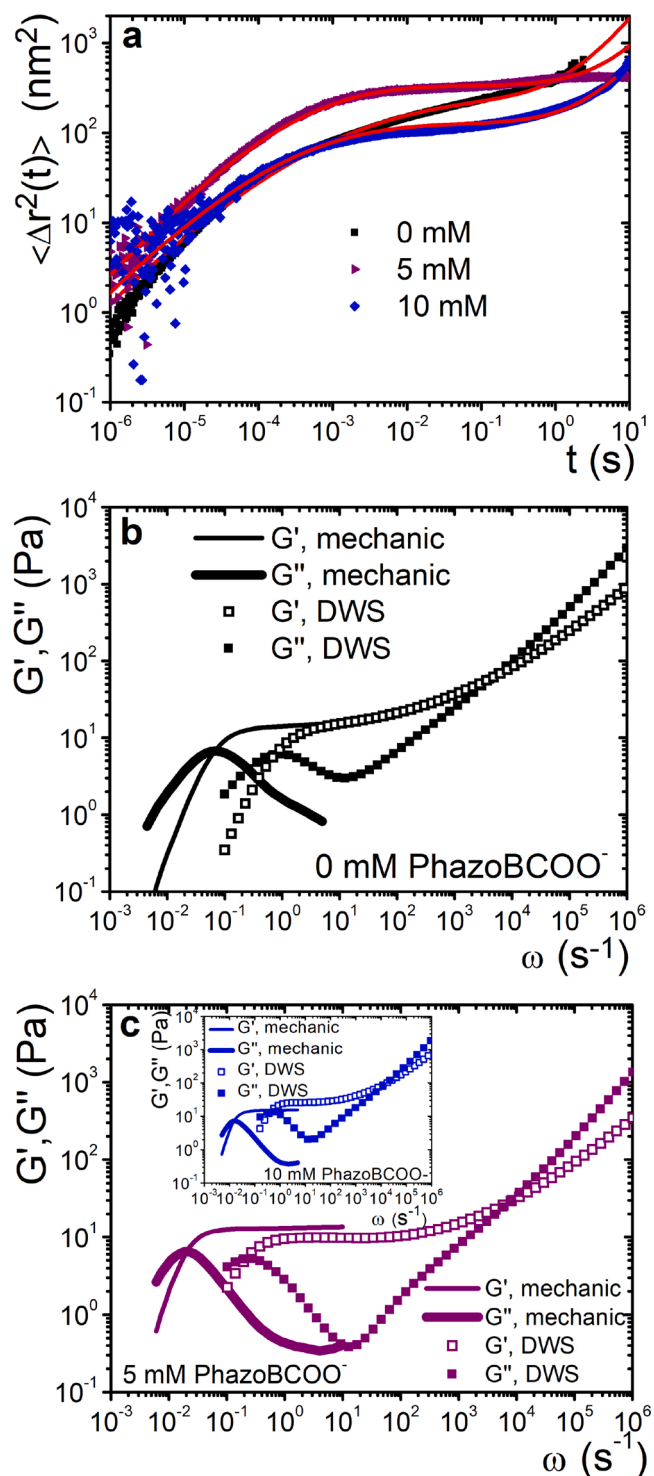


Fig. 5. a) MSD vs. t of tracers in WLM solutions made of TDPS/SDS/NaCl ($[TDPS] = 46$ mM, $R = 0.55$) with $C_{AZO} = 0, 5$, and 10 mM, at $T = 25$ °C and $pH = 12$; lines are fits to the Bellour et al model [20]. Viscoelastic spectra from mechanical rheometry and microrheology using DWS for the same T and pH described in (a). b) $C_{AZO} = 0$ mM, c) $C_{AZO} = 5$ mM, and in the inset $C_{AZO} = 10$ mM.

rheology, cell geometry, cell parameters, sample preparation, and even different reactive stocks have been described as factors that could introduce deviations in WLM rheology [33]. In mechanical rheology, it is not strange that measurements for different nominally identical samples have an error bar of ~ 20 % for G_o and ~ 5 % for τ_o . In DWS

microrheology, it is usual for a WLM sample measured in different days to has an error bar of $\sim 7\%$ for G_0 and $\sim 8\%$ for τ_0 [33]. Therefore, DWS microrheology seems to share some kind of these problems (sample preparation, probe particle dispersion method, etc.), so this has to be considered when DWS microrheology and mechanical rheology are compared. It has been suggested that mechanical experiments, where real and imaginary parts of $G^*(\omega)$ are obtained from the amplitude and phase shift of the response signal, are much more accurate than the DWS due to data treatment. Here, $\langle \Delta r^2(t) \rangle$ is measured in time-space, and residual effects of the polynomial fitting can produce small deviations during the Fourier transform to get $G'(\omega)$ and $G''(\omega)$. Then, a more significant error in the calculation of the crossing point is expected. Very recently, [34] it was reported possible problems of numerical nature, with the use of analytical continuation to go from the Laplace transform of the relaxation modulus to the frequency domain dynamic moduli. This issue affects the crossing region between $G'(\omega)$ and $G''(\omega)$. This issue will be analyzed in a forthcoming paper.

DWS microrheology reaches a bandwidth far beyond the conventional mechanical rheometry, allowing us to observe more features in the spectra, as two crossovers in $G^*(\omega)$, as presented in Fig. 5b, and Fig. 5c. Probe size and solvent inertial effects are negligible up to frequencies of $\omega \sim 10^6 \text{ s}^{-1}$. WLMs can be regarded as semiflexible chains at high frequencies, where the stress relaxes via intramicellar processes, as mentioned above. First dominated by the Rouse-Zimm modes, and then as frequency increases by the internal relaxation of individual Kuhn segments. Therefore, $|G^*(\omega)|$ exhibits a power-law behavior, $|G^*| \sim \omega^\nu$, with an exponent change from $\nu \sim 5/9$ to $\nu \sim 3/4$ that occurs at frequency ω_0 [21]. Fig. SM2 shows $|G^*|$ vs. ω for samples with $C_{AZO} = 0, 5$, and 10 mM .

Once G_0 , G_{min}^* , and ω_0 are obtained, the characteristic lengths (l_e , l_p , ξ , and L_C) can be calculated using the equations presented in section 2.6. Fig. 6a and b present these characteristic lengths as a function of C_{AZO} for the micellar solutions of TDPS/SDS/NaCl. In the case of the total contour length, L_C , in Fig. 6a, we also included for comparison how this length is modified in WLM solutions made of CTAB/NaSal/NaCl when PhazoBCOO⁻ is added, using the same experimental procedure [14]. The behavior of L_C in both systems is quite different. In CTAB/NaSal/NaCl, L_C decreases exponentially with the increase of C_{AZO} . However, in TDPS/SDS/NaCl, L_C increases to a maximum at $C_{AZO} \sim 5 \text{ mM}$. For 10 mM , L_C reaches the same value as the original micellar solution without chromophore. It is difficult to know if this declining trend is followed when more chromophore is added. However, according to the tendency

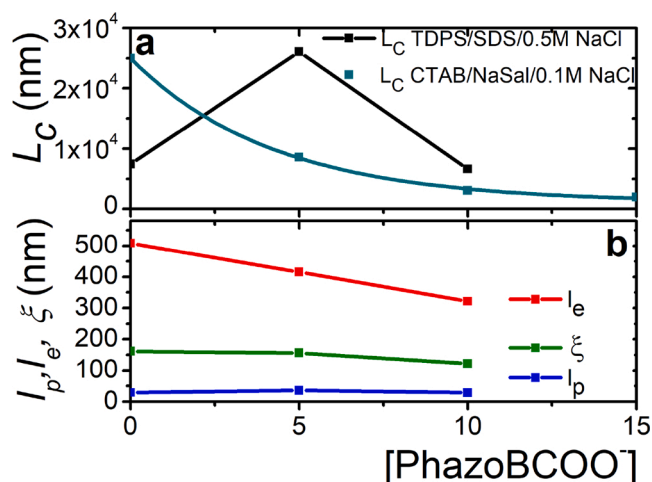


Fig. 6. Characteristic lengths L_C , l_e , l_p , and ξ , as a function of C_{AZO} for the micellar solutions of TDPS/SDS/NaCl ($[TDPS] = 46 \text{ mM}$, $R = 0.55$) at 25°C and $\text{pH} = 12$. a) L_C vs. C_{AZO} . Here, for comparison, it was included the data for the WLM solutions made of CTAB/NaSal/NaCl when PhazoBCOO⁻ is added from Ref. [14] b) l_e , l_p and ξ vs. C_{AZO} .

of τ_0 values as a function of C_{AZO} presented above, the contour length must decrease with further chromophore addition. Then, all seem to indicate that L_C continues to decline for concentrations larger than 10 mM . In Fig. 6b presents l_e , l_p , and mesh size ξ as a function of C_{AZO} . l_p and ξ almost do not significantly change with the increment of the PhazoBCOO⁻ concentration, but l_e decreases. The ratio L_C/l_e increases in samples where the chromophore is added, compared to the micellar solution without chromophore; for $C_{AZO} = 0, 5$, and 10 mM ; $L_C/l_e = 14.4, 62.5$, and 20.3 , respectively. There is more entanglement per average micelle, which could be one of the reasons why the viscosity increases at low $\dot{\gamma}$ in the samples with PhazoBCOO⁻. A larger entanglement hampers flow in micellar solutions with added chromophore concerning to the micellar solutions without chromophore.

3.4. ¹H-NMR and ¹H DOSY NMR

Experiments to determine the rheological behavior of the WLM solutions under discussion when PhazoBCOO⁻ is added are presented above. The tubular structure and dependence of the characteristic lengths of the micellar network on PhazoBCOO⁻ addition helped to explain some rheological results. However, Why do we observe such a low photoresponse of the rheological properties to the UV-irradiation? To look for an explanation, we develop ¹H-NMR experiments to get some clue about how the chromophore is embedded into the WLMs.

Fig. 7 (a) presents the ¹H-NMR spectrum of PhazoBCOO⁻ in deuterated water at $\text{pH} = 12$ (adding NaOD) and 25°C ; it agrees with the spectrum previously reported in Refs [11,35]. The other spectra in Fig. 7 correspond to micellar solutions where the chromophore is added; in (b) $C_{AZO} = 10 \text{ mM}$, and in (c) $C_{AZO} = 30 \text{ mM}$. Signals corresponding to TDPS and SDS appear at lower chemical shifts and are not shown here. The assigned proton signals in Fig. 7 correspond to the trans- (unprimed) and cis- (primed) isomers that are numbered according to the upper panel of Fig. 7. NMR signals agree with the integration ratio and spin-coupling among protons. In (a), signals of trans and cis-isomers can be observed. From this spectrum, the ratio of the cis/trans isomers can be

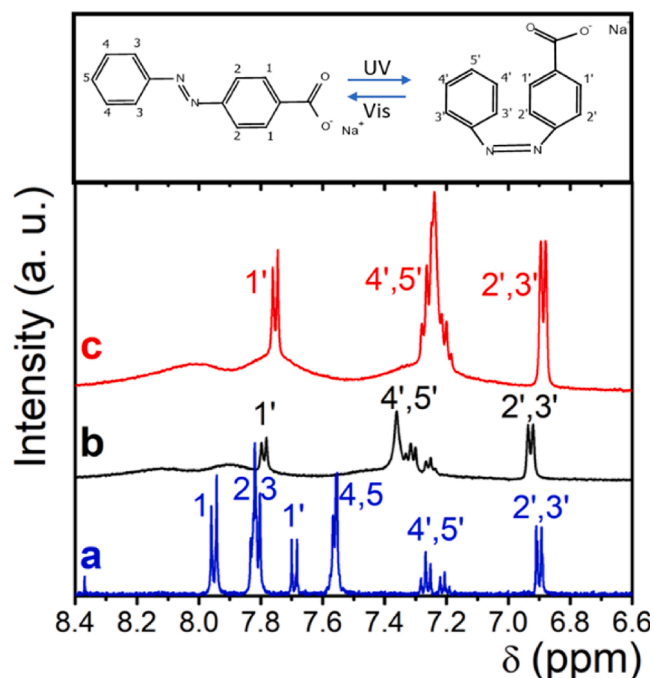


Fig. 7. ¹H-NMR spectra (500 MHz, D₂O, 25°C) of different solutions at $\text{pH} = 12$. Upper panel: Trans/cis structures with proton numbering. Lower panel: (a) Pure PhazoBCOO⁻; pH fixed with NaOD. (b) TDPS/SDS/NaCl ($[TDPS] = 46 \text{ mM}$, $R = 0.55$) with $C_{AZO} = 10 \text{ mM}$. (c) TDPS/SDS/NaCl ($[TDPS] = 46 \text{ mM}$, $R = 0.55$) at $C_{AZO} = 30 \text{ mM}$.

estimated using the integration signals for each isomer (~ 0.33). From the total quantity of PhazoBCOO⁻ in solution, a mole fraction of ~ 0.25 corresponds to the cis-isomer. In (b) and (c), the trans-isomer signals can not clearly be defined as in (a); the signals form small and broad bands ($\delta \sim 7.8\text{--}8.1$ ppm, and $\delta \sim 7.3\text{--}7.5$ ppm) probably correspond to the chromophore incorporation into the large WLM aggregates; we will go back to this issue below. In spectra (b) and (c), the 1' proton signal corresponding to the cis- isomer is slightly shifted to higher chemical shifts concerning spectrum (a). However, signals of protons 2', 3', 4', and 5' are almost at the same chemical shift.

The broad signals' intensity can be intensified to improve their identification, increasing temperature to induce more molecular mobility on the PhazoBCOO⁻ moiety. If the chromophore with a trans-conformation is incorporated into the micelles, its mobility could be low. The temperature of a couple of samples with different concentrations is increased up to $T=40^\circ\text{C}$. The results are in Fig. 8a and 8b; here, the spectrum at $T = 25^\circ\text{C}$ was also included for comparison, as well as their assigned proton signals for trans- and cis- isomers. As expected, the signal intensity corresponding to the trans-isomer increased as the temperature increases. In the case of $C_{\text{AZO}}=30$ mM (Fig. 8b), signals corresponding to the trans- and cis- isomers overlap. At 40°C , some signals are relatively broad, and others are sharp (cis- isomers); cis-isomer signals are not affected by temperature. These features can be

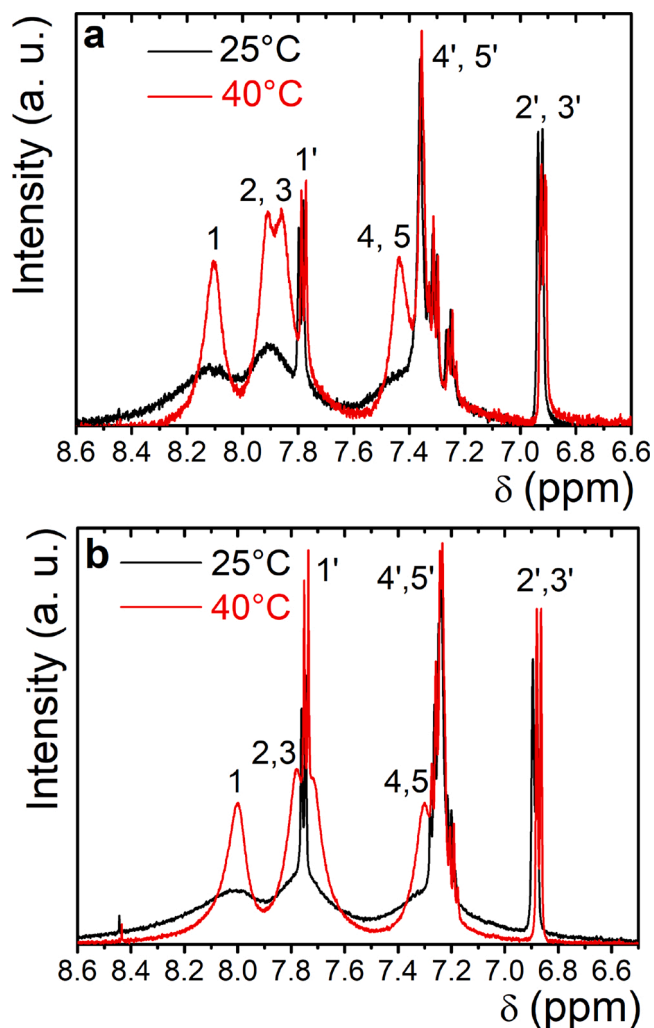


Fig. 8. ¹H-NMR spectra (500 MHz, D₂O) of micellar solutions of TDPS/SDS/NaCl ($[TDPS] = 46$ mM, $R = 0.55$) with added PhazoBCOO⁻ at two temperatures, $T = 25^\circ\text{C}$ and 40°C , ($p\text{H} = 12$ fixed with NaOD). a) $C_{\text{AZO}} = 10$ mM. b) $C_{\text{AZO}} = 30$ mM.

attributed to the cis- and trans- isomers' different chemical environments, suggesting that the trans- isomer is preferentially inside the micelles, while the cis-isomer is in the surrounding fluid outside the micelle. For $C_{\text{AZO}} = 10$ mM at 40°C , the integration of proton signals for each isomer yields a cis-/trans- ratio of ~ 0.55 , which corresponds to a cis-isomer mole fraction of ~ 0.35 . The reason to observe this high cis-isomer percentage is not evident because temperature induces the cis to trans isomerization [9]. After UV-irradiation, the cis-isomer is produced, the cis to trans isomerization occurs spontaneously in the dark due to the trans-isomer's thermodynamic stability, via thermal-induced or photo-induced isomerization. In azobenzene, the rate of thermal isomerization is found to be independent of solvent polarity [36]. In contrast, in azobenzene derivatives, the rate of thermal isomerization occurs at accelerated rates in a polar medium. In some way, probably related to the cis-isomer dipole moment, the TDPS and SDS surfactants' presence in a saline solution stabilizes and modifies this back isomerization of PhazoBCOO⁻.

Measurements of diffusion coefficient can be useful to determine the mobility of molecules in a mixture because they can be related to the size, mass, and structure of the surrounding environment of the diffusing molecules. ¹H DOSY NMR has been used for characterizing the molecular weight distributions in polymers, [37] to following mechanisms of polymerization [38], and in the determination of the critical micelle concentration in block-copolymer [39]. Also, the spectra of double-bonded cis- and trans-isomers with different molecular shapes but identical mass have been identified based on their diffusion coefficients due to their different tendencies to associate with or reverse micelles [40].

The self-diffusion coefficient of PhazoBCOO⁻ isomers in the system under study was estimated with ¹H DOSY NMR. Fig. 9a presents the results of the ¹H-DOSY-NMR experiment for the micellar solution of TDPS/SDS/NaCl with $C_{\text{AZO}} = 10$ mM at 40°C . In the upper side of the 2D DOSY diagram, we included the ¹H-NMR spectra of the WLM solution with the added chromophore; the diffusion peaks are on the left side, while the diffusion coefficient values are on the right side. If the two isomers were inside the micelle, we would expect a molecular diffusivity of the same order of magnitude for both isomers. The measured diffusion coefficient of the trans- and cis- isomers are $D = 8.35 \times 10^{-7} \text{ cm}^2/\text{s}$ and $D = 5.96 \times 10^{-6} \text{ cm}^2/\text{s}$, respectively. The diffusion coefficient difference between these isomers is little more than one order of magnitude. A molecular size change due to the trans-cis isomerization cannot explain such a high cis-diffusivity. Therefore, isomers' location seems to be in distinct surroundings; one isomer is outside the micelle, and the other one is inside it. This result is consistent with the cis-isomer being expelled from inside micelles, probably due to two factors. First, the micelle interior is highly hydrophobic, while the cis-isomer is a more polar molecule than the trans-isomer due to a molecular dipole moment. Therefore, it would be more stable and soluble in water. Moreover, its smaller size allows it to leave the micelle fast. The second factor is a geometrical one: the cis-isomer cannot fit nicely inside the micelle among relatively straight rods (linear tails) because isomerization involves rotation or inversion about the azo bond, with twisting of the phenyl rings, so that these rings are twisted at an angle of $\sim 90^\circ$. The surfactant packing factors will not fit to give the proper spontaneous curvature of the cylindrical micelle, and, consequently, the micelle would have to either change its spontaneous cylinder curvature, which is energetically expensive, or better, expel the undesired cis-molecule.

Fig. 9b shows the micellar solution's spectra with $C_{\text{AZO}} = 10$ mM, before and after 1 h of UV-irradiation at 25°C . After the UV-irradiation, the intensity of the peaks corresponding to the cis-isomer increases. UV-irradiation induces a trans-cis transition promoting the increase of the cis-isomer. However, as mentioned above, the cis-isomer is expelled out of the micelle. If cis-isomer had remained inside micelle on UV irradiation, this isomer's signals in the spectrum would have been observed as broad peaks and with a small change of chemical shift with respect to the spectrum before UV-irradiation. These events are not observed at 25°C .

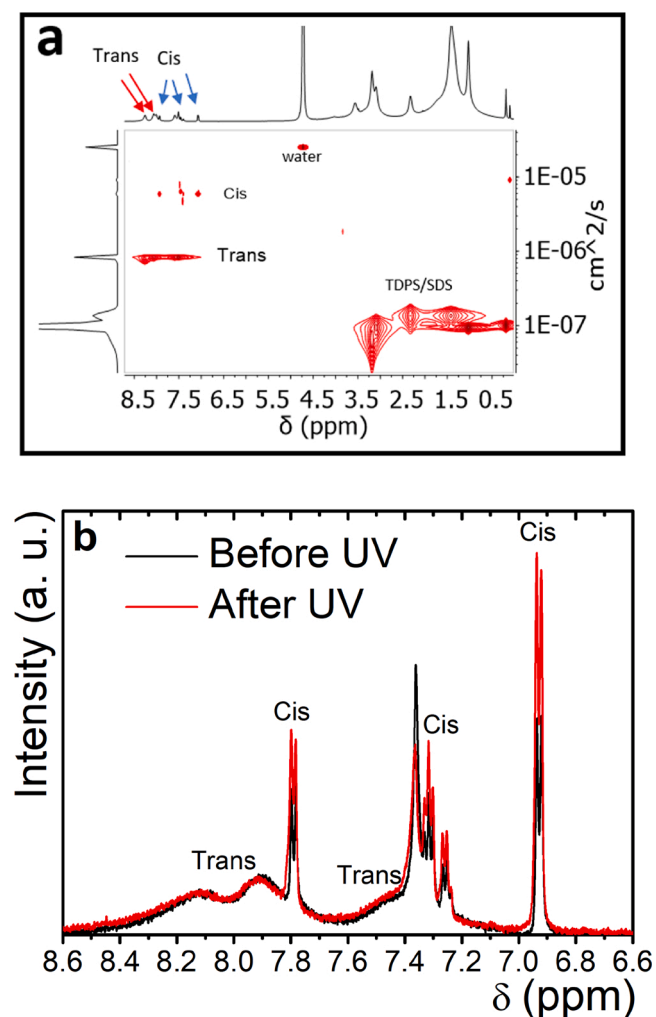


Fig. 9. a) $^1\text{H-NMR}$ DOSY (500 MHz, D_2O) for micellar solution of TDPS/SDS/NaCl ($[\text{TDPS}] = 46 \text{ mM}$, $R = 0.55$) with $C_{\text{AZO}} = 10 \text{ mM}$ at 40°C ($\text{pH} = 12$, fixed with NaOD). b) $^1\text{H-NMR}$ spectra for micellar solution of TDPS/SDS/NaCl ($[\text{TDPS}] = 46 \text{ mM}$, $R = 0.55$) with $C_{\text{AZO}} = 10 \text{ mM}$ at 25°C , before and after 1 h of UV-irradiation ($\text{pH} = 12$, fixed with NaOD).

The same effect was observed in a micellar system composed of a cationic Gemini surfactant and a cinnamate derivative. When the system is UV-irradiated, the cis-cinnamate escaped from the micellar layer [41]. The limited photoresponse to UV-irradiation of the WLM solutions under study here, when PhazoBCOO⁻ is added, can now be explained. From the quantity of PhazoBCOO⁻ (trans-isomer) incorporated in the micelles, some part is transformed into cis-isomer due to the UV-irradiation. However, this isomer goes out of the micelles. Therefore, small changes in the rheological properties must be expected with UV-irradiation.

4. Conclusion

Micellar solutions that self-assemble in WLMs when an azobenzene derivative is added can significantly change their rheological properties on UV-irradiation because the WLMs can be destroyed, or the micelles' size dramatically reduced. This occurs because of the photoswitchable molecule's conformation change due to a trans to cis isomerization, which involves rotation or inversion about the azo bond with twisting of the phenyl rings that alter the geometrical packing of the molecules involved in the micelle. However, despite containing photoswitchable molecules, the change of macroscopic properties in many systems is not significant after UV-irradiation. Some mechanisms prevent

chromophores with apparently good potential from having a good performance. Previously, we reported a system where as the chromophore concentration increases, it splits the micelles already before irradiation [14]. It was then not enough molecules embedded in the micelle with trans conformation to modify systems' flow properties on UV-irradiation. Here, we found another mechanism where the trans-isomer embedded in the micelles is converted into the cis-isomer on UV-irradiation. However, it is expelled from the micelles. Consequently, we observe a small change in the rheological properties of this micellar solution after UV-irradiation. One important conclusion is that much can be learned and used to design new photoswitchable mixtures by studying the chromophore-micelle interaction's physical chemistry and how the isomerization process occurs.

To study the interaction of 4-(phenylazo)benzoate ion with giant cylindrical micelles made of TDPS and SDS in saline water, we made rheological measurements to obtain the flow curves and the viscoelastic spectra at low and intermediate frequencies showing that the system at those frequencies behaves close to a Maxwellian fluid. Micro-rheological experiments with diffusive wave spectroscopy allowed us to obtain the system's high-frequency viscoelastic spectra; from this information, the characteristic length scales in the WLM network were estimated. We could show that the micelles' total contour length, when PhazoBCOO⁻ is present, first increases and then decreases when its concentration is varied, which is the same trend as the relaxation times, and low-shear viscosity. Also, since the ratio L_c/l_e increases in the micelle solutions increases as the chromophore is added, there is more entanglement per average micelle, which could be one reason why the viscosity increases at low $\dot{\gamma}$ in the samples with PhazoBCOO⁻. A larger entanglement hampers flow in micellar solutions with added chromophore as compared to the micellar solutions without chromophore. However, UV-irradiation had a small effect on rheological properties. The detailed interaction between the chromophore and the micelles was obtained with $^1\text{H-NMR}$ and ^1H DOSY NMR experiments; we determined what chromophore conformer was inside the micelles and the diffusivities of the isomers. The cis-isomer does not incorporate into the micelles; when it is formed inside them due to UV-irradiation, it is expelled. As mentioned above, the cis-isomer's expulsion from the micelle is the actual reason for observing a small change in the rheological properties after the micellar solution's UV-irradiation.

CRediT authorship contribution statement

Natalia Rincón-Londoño: Conceptualization. **Cristina Garza:** Conceptualization. **Nuria Esturau-Escofet:** Conceptualization. **Anna Kozina:** Conceptualization. **Rolando Castillo:** Conceptualization.

Declaration of Competing Interest

The authors declare that they have no known competing financial interests or personal relationships that could have appeared to influence the work reported in this paper.

Acknowledgments

Financial support from SEP-CONACyT (A1-S-15587) and DGAPA-UNAM (IN 106218) is gratefully acknowledged. We thank LURMN at IQUNAM with funds of CONACyT (0224747) for the NMR measurements, S. Tehuacanero-Cuapa, for his help in the acquisition of SEM images, Ricky Lopez for his help in optical rheometry, Dr. Antonio Tavera for his help in DWS, and S. Ramos for his technical support.

Appendix A. Supplementary data

Supplementary material related to this article can be found, in the online version, at doi:<https://doi.org/10.1016/j.colsurfa.2020.125903>.

References

- [1] D. Acharya, H. Kunieda, Wormlike micelles in mixed surfactant solutions, *Adv. Colloid Interface Sci.* 123 (2006) 401–413, <https://doi.org/10.1016/j.cis.2006.05.024>.
- [2] S. Ezrahi, E. Tuval, A. Aserin, Properties, main applications, and perspectives of worm micelles, *Adv. Colloid Interface Sci.* 128–130 (2006) 77–102, <https://doi.org/10.1016/j.cis.2006.11.017>.
- [3] C.A. Dreiss, Wormlike micelles: where do we stand? Recent developments, linear rheology and scattering techniques, *Soft Matter* 3 (2007) 956–970, <https://doi.org/10.1039/B705775J>.
- [4] J. Yang, Viscoelastic wormlike micelles and their applications, *Curr. Opin. Colloid Interface Sci.* 7 (2002) 276–281, [https://doi.org/10.1016/S1359-0294\(02\)00071-7](https://doi.org/10.1016/S1359-0294(02)00071-7).
- [5] S. Song, A. Song, J. Hao, Self-assembled structures of amphiphiles regulated via implanting external stimuli, *RSC Adv.* 4 (2014) 41864–41875, <https://doi.org/10.1039/C4RA04849K>.
- [6] Y. Hu, W. Zou, V. Julita, R. Ramanathan, R.F. Tabor, R. Nixon-Luke, G. Bryant, V. Bansal, B.L. Wilkinson, Photomodulation of bacterial growth and biofilm formation using carbohydrate-based surfactants, *Chem. Sci.* 7 (2016) 6628–6634, <https://doi.org/10.1039/C6SC03020C>.
- [7] S. Biswas, P. Kumari, P. Lakhani, B. Ghosh, Recent advances in polymeric micelles for anti-cancer drug delivery, *Eur. J. Pharm. Sci.* 83 (2016) 184–202, <https://doi.org/10.1016/j.ejps.2015.12.031>.
- [8] M. Yamada, M. Kondo, J. Mamiya, Y. Yu, M. Kinoshita, C. Barrett, T. Ikeda, Photomobile polymer materials: towards Light-Driven plastic motors, *Angew. Chem. Int. Edit.* 47 (2008) 4986–4988, <https://doi.org/10.1002/anie.200800760>.
- [9] E. Merino, M. Ribagorda, Control over molecular motion using the cis-trans photoisomerization of the azo group, *Beilstein J. Org. Chem.* 8 (2012) 1071–1090, <https://doi.org/10.3762/bjoc.8.119>.
- [10] J. García-Amorós, D. Velasco, Recent advances towards azobenzene-based light-driven real-time information-transmitting materials, *Beilstein J. Org. Chem.* 8 (2012) 1003–1017, <https://doi.org/10.3762/bjoc.8.113>.
- [11] Y. Bi, H. Wei, Q. Hu, W. Xu, Y. Gong, L. Yu, Wormlike micelles with photoresponsive viscoelastic behavior formed by surface active ionic liquid/azobenzene derivative mixed solution, *Langmuir* 31 (2015) 3789–3798, <https://doi.org/10.1021/acs.langmuir.5b00107>.
- [12] Y. Takahashi, Y. Yamamoto, S. Hata, Y. Kondo, Unusual viscoelasticity behavior in aqueous solutions containing a photoresponsive amphiphile, *J. Colloid Interface Sci.* 407 (2013) 370–374, <https://doi.org/10.1016/j.jcis.2013.06.010>.
- [13] H. Yan, Y. Long, K. Song, C. Tung, L. Zheng, Photo-induced transformation from wormlike to spherical micelles based on pyrrolidinium ionic liquids, *Soft Matter* 10 (2014) 115–121, <https://doi.org/10.1039/C3SM52346B>.
- [14] N. Rincón-Londoño, A. Tavera-Vázquez, C. Garza, N. Esturau-Escofet, A. Kozina, R. Castillo, Structural changes in wormlike micelles on the incorporation of small photoswitchable molecules, *J. Phys. Chem. B* 123 (2019) 9481–9490, <https://doi.org/10.1021/acs.jpcc.9b07276>.
- [15] T.G. Mason, Estimating the viscoelastic moduli of complex fluids using the generalized Stokes-Einstein equation, *Rheol. Acta* 39 (2000) 371–378, <https://doi.org/10.1007/s003970000094>.
- [16] J. Galvan-Miyoshi, J. Delgado, R. Castillo, Diffusing wave spectroscopy in Maxwellian fluids, *Eur. Phys. J. E* 26 (2008) 369–377, <https://doi.org/10.1140/epje/i2007-10335-8>.
- [17] S.A. Prahl, M. van Gemert, A.J. Welch, Determining the optical properties of turbid media by using the adding-doubling method, *App. Optics* 32 (1993) 559–568, <https://doi.org/10.1364/AO.32.000559>.
- [18] S.A. Prahl, Inverse Adding Doubling, 2017. <http://omlc.ogi.edu/software/iad/index.html>.
- [19] E. Sarmiento-Gomez, B. Morales-Cruzado, R. Castillo, Absorption effects in diffusing wave spectroscopy, *App. Optics* 53 (2014) 4675–4682, <https://doi.org/10.1364/AO.53.004675>.
- [20] M. Bellour, M. Skouri, J.-P. Munch, P. Hébraud, Brownian motion of particles embedded in a solution of giant micelles, *Eur. Phys. J. E* 8 (2002) 431–436, <https://doi.org/10.1140/epje/i2002-10026-0>.
- [21] N. Willenbacher, C. Oelschlaeger, M. Schopferer, P. Fischer, F. Cardinaux, F. Scheffold, Broad bandwidth optical and mechanical rheometry of wormlike micelle solutions, *Phys. Rev. Lett.* 99 (2007), 068302, <https://doi.org/10.1103/PhysRevLett.99.068302>.
- [22] W. Zou, R.G. Larson, A mesoscopic simulation method for predicting the rheology of semidilute wormlike micellar solutions, *J. Rheol.* 58 (2014) 681–721, <https://doi.org/10.1122/1.4868875>.
- [23] R. Granek, M. Cates, Stress relaxation in living polymers: results from a Poisson renewal model, *J. Chem. Phys.* 96 (1992) 4758–4767, <https://doi.org/10.1063/1.462787>.
- [24] R. Granek, Dip in $G''(\omega)$ of polymer melts and semidilute solutions, *Langmuir* 10 (1994) 1627–1629, <https://doi.org/10.1021/la00017a051>.
- [25] B. Arenas-Gómez, C. Garza, Y. Liu, R. Castillo, Alignment of wormlike micelles at intermediate and high shear rates, *J. Colloid Interface Sci.* 560 (2020) 618–625, <https://doi.org/10.1016/j.jcis.2019.10.052>.
- [26] Y. Tu, Q. Chen, Y. Shang, H. Teng, H. Liu, Photoresponsive behavior of wormlike micelles constructed by Gemini surfactant 12-3-12. 2Br- and different cinnamate derivatives, *Langmuir* 35 (2019) 4634–4645, <https://doi.org/10.1021/acs.langmuir.8b04290>.
- [27] M. Turner, M. Cates, Linear viscoelasticity of living polymers: a quantitative probe of chemical relaxation times, *Langmuir* 7 (1991) 1590–1594, <https://doi.org/10.1021/la00056a009>.
- [28] M. Cates, Reptation of living polymers: dynamics of entangled polymers in the presence of reversible chain-scission reactions, *Macromol* 20 (1987) 2289–2296, <https://doi.org/10.1021/ma00175a038>.
- [29] J.F. Berret, Transient rheology of wormlike micelles, *Langmuir* 13 (1997) 2227–2234, <https://doi.org/10.1021/la961078p>.
- [30] D. Lopez-Diaz, R. Castillo, The wormlike micellar solution made of a Zwitterionic surfactant (TDPS), an anionic surfactant (SDS), and brine in the semidilute regime, *J. Phys. Chem. B* 114 (2010) 8917–8925, <https://doi.org/10.1021/jp102108y>.
- [31] P.D. Olmsted, O. Radulescu, C.D. Lu, Johnson–Segalman model with a diffusion term in cylindrical Couette flow, *J. Rheol.* 44 (2000) 257–275, <https://doi.org/10.1122/1.551085>.
- [32] J. Delgado, R. Castillo, Shear-induced structures formed during thixotropic loops in dilute worm-micelle solutions, *J. Colloid Interface Sci.* 312 (2007) 481–488, <https://doi.org/10.1016/j.jcis.2007.03.010>.
- [33] E. Sarmiento-Gomez, D. Lopez-Diaz, R. Castillo, Microrheology and characteristic lengths in wormlike micelles made of a Zwitterionic surfactant and SDS in brine, *J. Phys. Chem. B* 114 (2010) 12193–12202, <https://doi.org/10.1021/jp104996h>.
- [34] Q. Li, X. Peng, D. Chen, G.B. McKenna, The Laplace approach in microrheology, *Soft Matter* 16 (2020) 3378–3383, <https://doi.org/10.1039/C9SM02242B>.
- [35] H. Oh, A. Ketner, R. Heymann, E. Kesselman, D. Danino, D. Falvey, S. Raghavan, A simple route to fluids with photoswitchable viscosities based on a reversible transition between vesicle and wormlike micelles, *Soft Matter* 9 (2013) 5025–5033, <https://doi.org/10.1039/C3SM00070B>.
- [36] N.K. Joshi, M. Fuyuki, A. Wada, Polarity controlled reaction path and kinetics of thermal Cis-to-Trans isomerization of 4-Aminoazobenzene, *J. Phys. Chem. B* 118 (2014) 1891–1899, <https://doi.org/10.1021/jp4125205>.
- [37] C. Johnson Jr., Diffusion ordered nuclear magnetic resonance spectroscopy: principles and applications, *Prog. Nucl. Mag. Res. Sp.* 34 (1999) 203–256, [https://doi.org/10.1016/S0079-6565\(99\)00003-5](https://doi.org/10.1016/S0079-6565(99)00003-5).
- [38] N. Cherifi, A. Khoukh, A. Benaboura, L. Billon, Diffusion-ordered spectroscopy NMR DOSY: an all-in-one tool to simultaneously follow side reactions, livingness and molar masses of polymethylmethacrylate by nitroxide mediated polymerization, *Polym. Chem.* 7 (2016) 5249–5257, <https://doi.org/10.1039/C6PY00927A>.
- [39] Y. Bakkour, V. Darcos, S. Lia, J. Coudane, Diffusion ordered spectroscopy (DOSY) as a powerful tool for amphiphilic block copolymer characterization and for critical micelle concentration (CMC) determination, *Polym. Chem.* 3 (2012) 2006–2010, <https://doi.org/10.1039/C2PY20054F>.
- [40] S.R. Chandhari, N. Suryaprakash, Diffusion ordered spectroscopy for resolution of double bonded cis, trans-isomers, *J. Mol. Struct.* 1017 (2012) 106–108, <https://doi.org/10.1016/j.molstruc.2012.03.009>.
- [41] Y. Tu, Z. Ye, C. Lian, Y. Shang, H. Teng, H. Liu, UV-responsive behavior of multistate and multiscale self-assemblies constructed by Gemini surfactant 12-3-12.2 Br- and trans-o-methoxy-cinnamate, *Langmuir* 34 (2018) 12990–12999, <https://doi.org/10.1021/acs.langmuir.8b02914>.